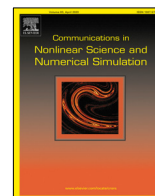




Contents lists available at ScienceDirect

Communications in Nonlinear Science and Numerical Simulation

journal homepage: www.elsevier.com/locate/cnsns

Chaotic discrete breathers and their effect on macroscopic properties of triangular lattice

A. Upadhyaya^{a,1}, M.N. Semenova^{b,1}, A.A. Kudreyko^{c,1}, S.V. Dmitriev^{d,e,1,*}^a Indian Institute of Technology Kharagpur, Kharagpur 721302, India^b Polytechnic Institute (Branch) in Mirny, North-Eastern Federal University, Tikhonova St. 5/1, 678170 Mirny, Sakha Republic (Yakutia), Russia^c Department of Medical Physics and Informatics, Bashkir State Medical University, Lenin St. 3, 450008 Ufa, Russia^d Institute of Molecule and Crystal Physics, Ufa Federal Research Centre of RAS, Ufa 450054, Russia^e Ufa State Petroleum Technological University, Ufa 450062, Russia

ARTICLE INFO

Article history:

Available online 26 April 2022

Keywords:

Nonlinear lattice

Delocalized nonlinear vibrational mode

Discrete breather

Macroscopic properties

ABSTRACT

The localization of energy on chaotic discrete breathers (DBs) arising in a two-dimensional triangular lattice due to the modulation instability of delocalized nonlinear vibrational modes (DNVMs) is analyzed. Three DNVMs with frequencies above the phonon band and demonstrating hard-type anharmonicity (an increase in the vibration frequency with amplitude) are considered. Chaotic DBs have long lifetime, slowly radiate their energy and eventually disappear. The evolution of the macroscopic characteristics of the lattice is observed during the transition from the regime with chaotic DBs to thermal equilibrium. It is established that chaotic DBs with a hard type of anharmonicity reduce the ratio of the total energy to the kinetic energy (and, consequently, reduce the heat capacity). They also reduce lattice pressure at constant area (and therefore reduce thermal expansion). The tensile rigidity of the lattice also decreases due to DBs with a hard type of anharmonicity. The most sensitive to the presence of DBs is the pressure, which in the presence of DBs is approximately 30% less than in thermal equilibrium. The ratio of the total energy to the kinetic energy in the regime of chaotic DBs decreases by about 3%, and the tensile rigidity by only 0.1%.

© 2022 Elsevier B.V. All rights reserved.

1. Introduction

In the works of theorists, it was shown that nonlinear lattices can support spatially localized vibrational modes called discrete breathers (DBs) or intrinsic localized modes [1,2]. DBs have been extensively studied over the past three decades, which is reflected in review articles [3–5]. The existence of DBs in crystal lattices have been confirmed experimentally [6–11] and in a number of molecular dynamics [12–21] as well as in some first-principles simulations [22,23].

It is interesting how DBs affect the macroscopic properties of crystals. Probably the first systematic discussion of this issue was by Manley [24] based on experimental results available at that time [6–8]. Simulation results obtained for nonlinear chains also confirmed that DBs reduce thermal conductivity by scattering phonons [25,26], affect heat

* Corresponding author at: Institute of Molecule and Crystal Physics, Ufa Federal Research Centre of RAS, Ufa 450054, Russia.

E-mail addresses: abhisekupadhyaya23@gmail.com (A. Upadhyaya), mariya_semyonova86@mail.ru (M.N. Semenova), alexkudreyko@mail.ru (A.A. Kudreyko), dmitriev. sergey.v@gmail.com (S.V. Dmitriev).

¹ The authors have equally contributed to this study.

capacity [27,28], thermal expansion and elastic constants [28]. In the present study the effect of DBs on macroscopic properties of a two-dimensional nonlinear lattice is addressed.

Our approach is similar to that used in previous works [27,28]. It is based on the fact that short-wavelength delocalized nonlinear vibrational modes (DNVMs) with frequencies outside the phonon spectrum of the lattice experience modulational instability, which leads to the formation of chaotic DBs [29–38]. DNVMs of triangular lattice were described in the work [39], where it was shown that there are three of them with frequencies above the phonon spectrum. DBs in triangular lattice with Fermi–Pasta–Ulam–Tsingou (FPUT) potential, obtained by imposing localizing functions upon DNVMs with frequencies above the phonon band, were described in the work [40], and some of them were previously known [38].

Chaotic DBs gradually lose energy due to the excitation of phonons, and the lattice approaches the state of thermal equilibrium. Comparison of macroscopic parameters of the lattice with chaotic DBs and in thermal equilibrium makes it possible to understand how DBs affect macroscopic properties.

The following is a description of the triangular β -FPUT lattice and three DNVMs with frequencies above the phonon band (Section 2). The macroscopic properties of the lattice are then introduced, including specific heat, mean pressure (associated with thermal expansion) and elastic constants (Section 2). The simulation results include the time variation of macroscopic properties during the development of modulation instability of the DNVMs, leading to the appearance of chaotic DBs, their evolution and disappearance (Section 5). Based on the results obtained, a conclusion is drawn about the effect of the hard type anharmonicity DBs on the macroscopic properties of the triangular β -FPUT lattice (Section 6).

2. Nonlinear triangular lattice and its dispersion relation

A two-dimensional triangular β -FPUT lattice with nearest neighbor interactions is considered. A lattice is defined as a set of points in the xy plane that have radius-vectors

$$\xi_{i,j} = i\mathbf{e}_1 + j\mathbf{e}_2, \tag{1}$$

where i and j are integers and the basis of the lattice can be defined by the vectors $\mathbf{e}_1 = (h, 0)$ and $\mathbf{e}_2 = (h/2, h\sqrt{3}/2)$, where h is the distance between the nearest lattice points.

Each particle has two degrees of freedom, the components of the displacement vector $(u_{i,j}, v_{i,j})$, which are unknown functions of time. Position of the particle i, j is given by the radius vector $\mathbf{r}_{i,j} = \xi_{i,j} + (u_{i,j}, v_{i,j})$.

Each particle interacts with the six nearest neighbors via the β -FPUT potential

$$\varphi(r) = \frac{k}{2}(r - h)^2 + \frac{\beta}{4}(r - h)^4, \tag{2}$$

where r is the distance between the particles, k and β are the coefficients for the harmonic and anharmonic parts of the potential, respectively. We take $h = 1$ and $k = 1$ (choosing the units of distance and energy, respectively) and set $\beta = 10$, for which the nonlinearity effects become noticeable for particle displacements of the order of 0.1. Particle mass is set equal to $m = 1$ by choosing a unit of time.

Computational cell that includes $I \times J$ particles is considered. Periodic boundary conditions are used, $\mathbf{r}_{i,j} = \mathbf{r}_{i+I,j} = \mathbf{r}_{i,j+J}$. The vectors connecting the six nearest neighbors with the i, j particle are:

$$\begin{aligned} \mathbf{R}_{i,j,1} &= \mathbf{r}_{i+1,j} - \mathbf{r}_{i,j}, & \mathbf{R}_{i,j,2} &= \mathbf{r}_{i,j+1} - \mathbf{r}_{i,j}, \\ \mathbf{R}_{i,j,3} &= \mathbf{r}_{i-1,j+1} - \mathbf{r}_{i,j}, & \mathbf{R}_{i,j,4} &= \mathbf{r}_{i-1,j} - \mathbf{r}_{i,j}, \\ \mathbf{R}_{i,j,5} &= \mathbf{r}_{i,j-1} - \mathbf{r}_{i,j}, & \mathbf{R}_{i,j,6} &= \mathbf{r}_{i+1,j-1} - \mathbf{r}_{i,j}. \end{aligned} \tag{3}$$

The Hamiltonian (total energy) of the computational cell is the sum of the kinetic and potential energies:

$$H = K + P = \sum_{i=1}^I \sum_{j=1}^J \frac{m}{2} (\dot{\mathbf{r}}_{i,j}, \dot{\mathbf{r}}_{i,j}) + \frac{1}{2} \sum_{i=1}^I \sum_{j=1}^J \sum_{k=1}^6 \varphi(|\mathbf{R}_{i,j,k}|), \tag{4}$$

where overdot means differentiation with respect to time.

With the help of the Hamilton's equation, from the Hamiltonian Eq. (4) one can derive the following equations of motion

$$\begin{aligned} m\ddot{u}_{i,j} &= \sum_{k=1}^6 \frac{\varphi'(|\mathbf{R}_{i,j,k}|)}{|\mathbf{R}_{i,j,k}|} R_{i,j,k,x}, \\ m\ddot{v}_{i,j} &= \sum_{k=1}^6 \frac{\varphi'(|\mathbf{R}_{i,j,k}|)}{|\mathbf{R}_{i,j,k}|} R_{i,j,k,y}. \end{aligned} \tag{5}$$

For small displacements, $u_{i,j} \ll h$, $v_{i,j} \ll h$ the following linearized equations of motion can be obtained from Eq. (5):

$$m\ddot{u}_{i,j} = k(u_{i-1,j} - 2u_{i,j} + u_{i+1,j})$$

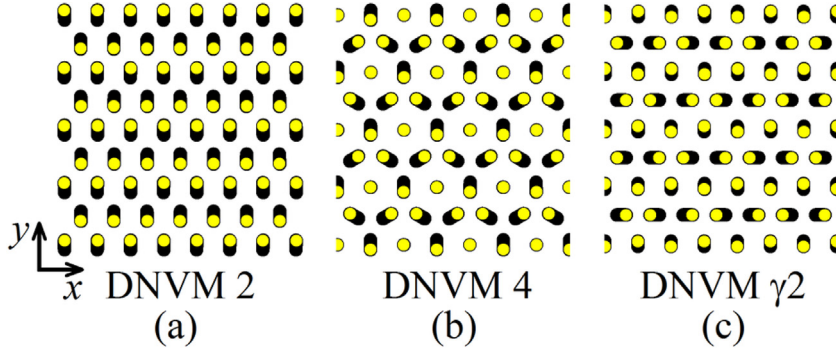


Fig. 1. Three DNVMs of the triangular lattice having frequencies above the phonon band [39]. Particles are shown in yellow and their trajectories in black. The particles are shown at the moment of maximum deviation from the lattice positions. In (a), all particles oscillate along the y axis with the amplitude A . In (b), all oscillating particles have the vibration amplitude A . One quarter of the particles are at rest. In (c), particles oscillating along the x axis (y axis) have vibration amplitude equal to A (B).

$$\begin{aligned}
 & + \frac{k}{4}[u_{i,j+1} - u_{i,j} + \sqrt{3}(v_{i,j+1} - v_{i,j})] \\
 & + \frac{k}{4}[u_{i-1,j+1} - u_{i,j} - \sqrt{3}(v_{i-1,j+1} - v_{i,j})] \\
 & + \frac{k}{4}[u_{i,j-1} - u_{i,j} + \sqrt{3}(v_{i,j-1} - v_{i,j})] \\
 & + \frac{k}{4}[u_{i+1,j-1} - u_{i,j} - \sqrt{3}(v_{i+1,j-1} - v_{i,j})], \tag{6}
 \end{aligned}$$

$$\begin{aligned}
 m\ddot{v}_{i,j} = & \frac{k\sqrt{3}}{4}[u_{i,j+1} - u_{i,j} + \sqrt{3}(v_{i,j+1} - v_{i,j})] \\
 & - \frac{k\sqrt{3}}{4}[u_{i-1,j+1} - u_{i,j} - \sqrt{3}(v_{i-1,j+1} - v_{i,j})] \\
 & + \frac{k\sqrt{3}}{4}[u_{i,j-1} - u_{i,j} + \sqrt{3}(v_{i,j-1} - v_{i,j})] \\
 & - \frac{k\sqrt{3}}{4}[u_{i+1,j-1} - u_{i,j} - \sqrt{3}(v_{i+1,j-1} - v_{i,j})]. \tag{7}
 \end{aligned}$$

Substituting into Eqs. (6) and (7) the solution in the form of small-amplitude waves, $u_{i,j} = F \exp[\mathbf{i}(qi + pj - \omega t)]$ and $v_{i,j} = B \exp[\mathbf{i}(qi + pj - \omega t)]$, where \mathbf{i} is imaginary unit, one obtains the dispersion relation [40]

$$\omega_{1,2}^2(q, p) = \frac{-\xi \pm \sqrt{\xi^2 - 16m^2\gamma}}{8m^2}, \tag{8}$$

where

$$\begin{aligned}
 \xi & = 8mk(S + \cos q - 1), \\
 \gamma & = 3k^2[4(\cos q - 1)S + S^2 - Q^2], \\
 S & = \cos p + \cos(q - p) - 2, \\
 Q & = \cos p - \cos(q - p). \tag{9}
 \end{aligned}$$

It is important to know the highest phonon frequency. As mentioned above, in this study we take $k = m = 1$, then the maximum frequency is $\omega_{\max} = \sqrt{6}$, which is observed for the following wave numbers of the first Brillouin zone: $(q, p) = (\pm\pi, \pm\pi)$, $(q, p) = (\pm\pi, 0)$, and $(q, p) = (0, \pm\pi)$.

3. Delocalized modes having frequencies above the phonon band

The initial conditions are set to excite one of the three DNVMs shown in Fig. 1. These modes have frequencies above the phonon band and are designated as in the original work [39]. In (a) and (b) the one-component DNVMs are shown. Initial displacement vectors of all moving particles have the same length A , which is the mode amplitude. In (c) the DNVM has two components, particles moving along x (along y) axis have initial displacement vectors of length A (of length B).

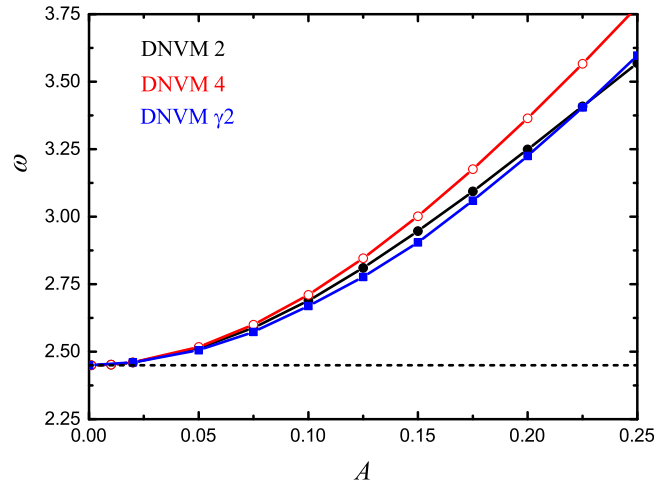


Fig. 2. Frequency as the function of amplitude for DNVM 2 (black dots), DNVM 4 (red circles) and DNVM $\gamma 2$ (blue squares). The highest phonon frequency is shown by the horizontal dashed line.

Initial velocities of all particles in all three modes are equal to zero, $\dot{r}_{i,j}^0 = 0$. Thus, the initial displacements are expressed as follows:

For DNVM 2

$$u_{i,j}^0 = 0, \quad v_{i,2j}^0 = A, \quad v_{i,2j+1}^0 = -A. \tag{10}$$

For DNVM 4

$$\begin{aligned} u_{2i,2j}^0 &= 0, \quad v_{2i,2j}^0 = 0, \quad u_{2i+1,2j}^0 = 0, \\ v_{2i+1,2j}^0 &= -A, \quad u_{2i,2j+1}^0 = -u_{2i+1,2j+1}^0 = -A\sqrt{3}/2, \\ v_{2i,2j+1}^0 &= v_{2i+1,2j+1}^0 = A/2. \end{aligned} \tag{11}$$

For DNVM $\gamma 2$

$$\begin{aligned} u_{2i,2j}^0 &= A, \quad u_{2i+1,2j}^0 = -A, \quad v_{i,2j}^0 = 0, \\ u_{i,2j+1}^0 &= 0, \quad v_{2i,2j+1}^0 = -B, \quad v_{2i+1,2j+1}^0 = B. \end{aligned} \tag{12}$$

Generally speaking, the two components of DNVM $\gamma 2$ have incommensurate frequencies, but the amplitudes A and B can be chosen so that the frequencies of both components become equal [40]. For the model parameters used in this study and for the amplitudes considered in this study, the frequencies are equal for $A = 0.02, B = 0.572A; A = 0.03, B = 0.5658A$ and $A = 0.04, B = 0.557438A$. In the limit $A \rightarrow 0$ one has $B \rightarrow A/\sqrt{3}$ [40].

We excite DNVMs using the initial conditions described above and integrate the nonlinear equations of motion (5) using the Störmer symplectic integrator of order six [41] with the time step of 10^{-3} time units.

The oscillation period T of the DNVM is found from the time dependence of the particle coordinates. Then the oscillation frequency is equal to $\omega = 2\pi/T$.

In Fig. 2 one can see DNVM frequency as the function of amplitude. Result for DNVM 2 is shown by the black dots, for DNVM 4 by the red circles, and for DNVM $\gamma 2$ by the blues squares. The upper edge of the phonon spectrum, $\omega_{\max} = \sqrt{6} \approx 2.45$, is shown by the horizontal dashed line. In the $A \rightarrow 0$ limit, DNVMs transform into low-amplitude phonons with a frequency at the upper edge of the phonon spectrum. The DNVM frequencies increase with increasing amplitude due to hard-type anharmonicity.

We are interested in DNVMs with frequency above the phonon spectrum, since for a modulationally unstable DNVM there is no direct channel for transferring its energy to delocalized phonons, since it does not resonate with any phonon. Consequently, as a result of the modulational instability of such a DNVM, energy is localized in the form of discrete breathers [29].

4. Macroscopic properties of the lattice

Let us describe some macroscopic properties of the lattice.

The lattice kinetic energy K oscillates over time and we will consider the time averaged value

$$\langle K \rangle = \frac{1}{\tau} \int_0^\tau K dt, \tag{13}$$

where $\tau = 5T$ and $T = 2\pi/\sqrt{6}$ is the period of the highest frequency phonon.

Let us analyze the ratio of the total to the time-averaged kinetic energy of the system,

$$C_V = \frac{H}{\langle K \rangle}. \quad (14)$$

The notation used for this ratio will be rationalized later. For a harmonic lattice, $C_V = 2$, since in this case $\langle K \rangle = H/2$. On the other hand, the anharmonicity of the lattice leads to a deviation of C_V from the value 2. This means that C_V characterizes the anharmonicity of the vibrational mode.

Components of the mechanical stress tensor can be calculated as follows

$$\begin{aligned} \sigma_{xx} &= \frac{1}{S} \sum_{i=1}^I \sum_{j=1}^J \sum_{k=1}^3 \frac{\varphi'(|\mathbf{R}|)}{|\mathbf{R}|} R_x^2, \\ \sigma_{yy} &= \frac{1}{S} \sum_{i=1}^I \sum_{j=1}^J \sum_{k=1}^3 \frac{\varphi'(|\mathbf{R}|)}{|\mathbf{R}|} R_y^2, \\ \sigma_{xy} &= \frac{1}{S} \sum_{i=1}^I \sum_{j=1}^J \sum_{k=1}^3 \frac{\varphi'(|\mathbf{R}|)}{|\mathbf{R}|} R_x R_y, \end{aligned} \quad (15)$$

where $\mathbf{R}_{i,j,k} = (R_{i,j,k,x}, R_{i,j,k,y})$ and we used short notations $\mathbf{R} \equiv \mathbf{R}_{i,j,k}$, $R_x \equiv R_{i,j,k,x}$, $R_y \equiv R_{i,j,k,y}$; $S = (\sqrt{3}/2)h^2IJ$ is the area of the computational cell.

The Hooke's law under plane stress conditions has the form

$$\begin{aligned} \sigma_{xx} &= C_{11}\varepsilon_{xx} + C_{12}\varepsilon_{yy} + C_{13}\varepsilon_{xy}, \\ \sigma_{yy} &= C_{21}\varepsilon_{xx} + C_{22}\varepsilon_{yy} + C_{23}\varepsilon_{xy}, \\ \sigma_{xy} &= C_{31}\varepsilon_{xx} + C_{32}\varepsilon_{yy} + C_{33}\varepsilon_{xy}, \end{aligned} \quad (16)$$

where ε_{xx} , ε_{yy} and ε_{xy} are components of the strain tensor and $C_{ij} = C_{ji}$ are the stiffness constants.

The following two stiffness constants will be analyzed:

$$\begin{aligned} C_{11} &= \frac{1}{S} \sum_{i=1}^I \sum_{j=1}^J \sum_{k=1}^3 \left(\frac{\varphi''(|\mathbf{R}|)}{|\mathbf{R}|^2} - \frac{\varphi'(|\mathbf{R}|)}{|\mathbf{R}|^3} \right) R_x^4, \\ C_{22} &= \frac{1}{S} \sum_{i=1}^I \sum_{j=1}^J \sum_{k=1}^3 \left(\frac{\varphi''(|\mathbf{R}|)}{|\mathbf{R}|^2} - \frac{\varphi'(|\mathbf{R}|)}{|\mathbf{R}|^3} \right) R_y^4. \end{aligned} \quad (17)$$

If the lattice particles vibrate, then the stresses and stiffness constants are functions of time. These characteristics will be averaged over time,

$$\langle \sigma_{ij} \rangle = \frac{1}{\tau} \int_0^\tau \sigma_{ij}(t) dt, \quad \langle C_{ij} \rangle = \frac{1}{\tau} \int_0^\tau C_{ij}(t) dt, \quad (18)$$

where $\tau = 5T$ and $T = 2\pi/\sqrt{6}$ is the period of the highest frequency phonon.

Averaged over time mean stress is

$$\langle p \rangle = \frac{1}{2} (\langle \sigma_{xx} \rangle + \langle \sigma_{yy} \rangle). \quad (19)$$

Averaged over time stiffness of the lattice will be characterized by

$$\langle C \rangle = \frac{1}{2} (\langle C_{11} \rangle + \langle C_{22} \rangle). \quad (20)$$

Note that C_{11} and C_{22} are the stiffness coefficients for tension/compression along the x and y axis, respectively.

Unless otherwise stated, the calculations consider a lattice of size $I = J = 192$ with a total number of particles of 36,864.

The degree of energy localization in the lattice can be quantified using the following localization parameter:

$$L = IJ \frac{\sum_i \sum_j e_{i,j}^2}{\left(\sum_i \sum_j e_{i,j} \right)^2}, \quad (21)$$

where $e_{i,j}$ is the total (kinetic plus potential) energy of the i, j particle. If the energy is distributed equally among all particles, then $L = 1$. If all the energy is localized on a single particle, then $L = IJ$, which is the total number of particles in the computational cell.

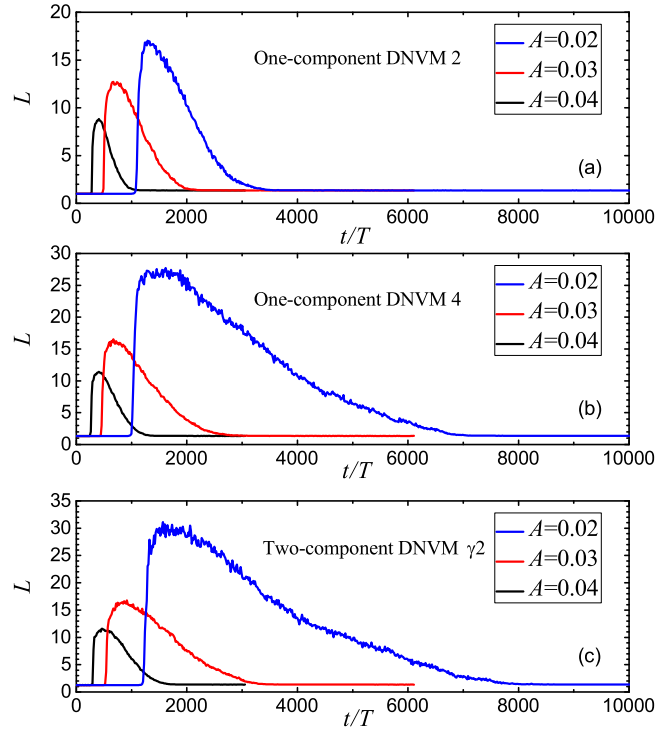


Fig. 3. Localization parameter as the function of time normalized to the period of the highest frequency phonon mode $T = 2\pi/\sqrt{6}$ (approximately equal to the DB period). Results for (a) DNVM 2, (b) DNVM 4 and (c) DNVM $\gamma 2$, and for the three DNVM amplitudes: $A = 0.02$ (blue lines), $A = 0.03$ (red lines) and $A = 0.04$ (black lines).

5. Simulation results

We excite the three investigated DNVMs with three amplitudes: $A = 0.02, 0.03$ and 0.04 . These amplitudes exceed the minimum value at which DNVMs are stable, and, as shown below, modulational instability leads to the formation of chaotic DBs with a large but finite lifetime. Let us analyze the time evolution of the localization parameter and the macroscopic characteristics of the lattice.

In Fig. 3, time evolution of the localization parameter Eq. (21) is presented for (a) DNVM 2, (b) DNVM 4 and (c) DNVM $\gamma 2$. Blue, red and black lines show the results for the DNVM amplitudes $A = 0.02, 0.03$ and 0.04 , respectively. Time is normalized to the period of the phonon mode having maximal frequency, $T = 2\pi/\sqrt{6}$. The period of DBs is somewhat less than T , since their frequencies lie above the phonon band. This means that T can be viewed as a DB period. The results shown in Fig. 3 indicate that with decreasing A , the development of modulation instability slows down, and chaotic DBs have a longer lifetime. The shortest lifetime have DBs arising from DNVM 2 and the longest – from DNVM $\gamma 2$.

It is instructive to see how the maximum energy in a system changes over time. This is shown in Fig. 4, where $e_{i,j}^{\max}$ is the maximum total energy of the particles. It can be seen that $e_{i,j}^{\max}$ is small during the development of the instability of the DNVM, then sharply increases with the formation of chaotic DBs and remains high during the lifetime of the DBs, and, finally, becomes small when thermal equilibrium is reached. The maximum energy is higher for larger A , but, as already mentioned, the DB lifetime is higher for smaller A .

Initially, the energy is homogeneously distributed over the lattice. The development of modulation instability leads to energy localization. The kinetics of energy localization is shown in Fig. 5 for (a) DNVM 2, (b) DNVM 4 and (c) DNVM $\gamma 2$, in all cases $A = 0.03$. Only in this case, a small size of the computational cell is used ($I = J = 48$). Black (white) color corresponds to the minimum (maximum) energy. The left (right) panels show the energy distribution over the computational cell at the time when, with an increase in the localization parameter, the value $L = 0.8L^{\max}$ ($L = L^{\max}$) is reached. In the right panels highly localized DBs can be seen.

We now turn to a discussion of the influence of chaotic DBs on the macroscopic properties of the triangular β -FPUT lattice.

In Fig. 6, time evolution of the ratio of the total to the time-averaged kinetic energy, Eq. (14), is shown for (a) DNVM 2, (b) DNVM 4 and (c) DNVM $\gamma 2$. The blue, red and black curves show the results for $A = 0.02, 0.03$ and 0.04 , respectively. The ratio in thermal equilibrium is higher than in the case when chaotic DBs exist in the lattice. We conclude that DBs reduce the ratio of total to kinetic energy of the lattice.

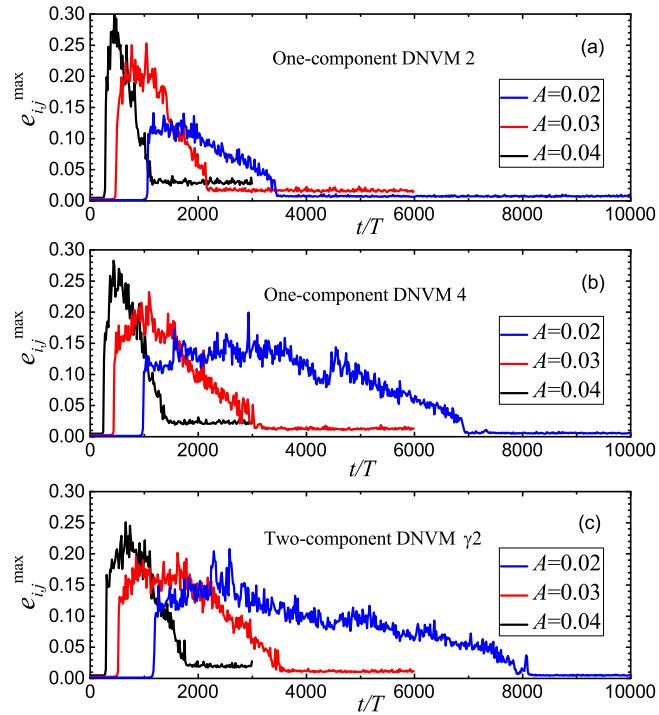


Fig. 4. Dependence of the maximum total energy of the particles on time for (a) DNVM 2, (b) DNVM 4 and (c) DNVM $\gamma 2$. The blue, red and black curves show the results for $A = 0.02$, 0.03 and 0.04 , respectively. Time is normalized to the period of phonon with maximal frequency, which is close to the period of DB.

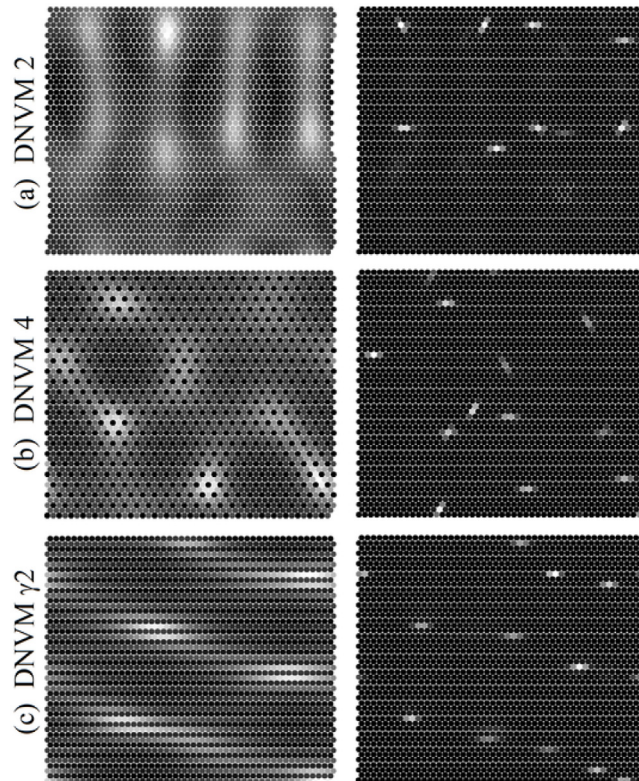


Fig. 5. Development of modulational instability of (a) DNVM 2, (b) DNVM 4 and (c) DNVM $\gamma 2$; results for $A = 0.03$. Left (right) panels show distribution of energy over lattice at the time when $L = 0.8L^{\max}$ ($L = L^{\max}$). Black (white) color corresponds to the minimal (maximal) energy.

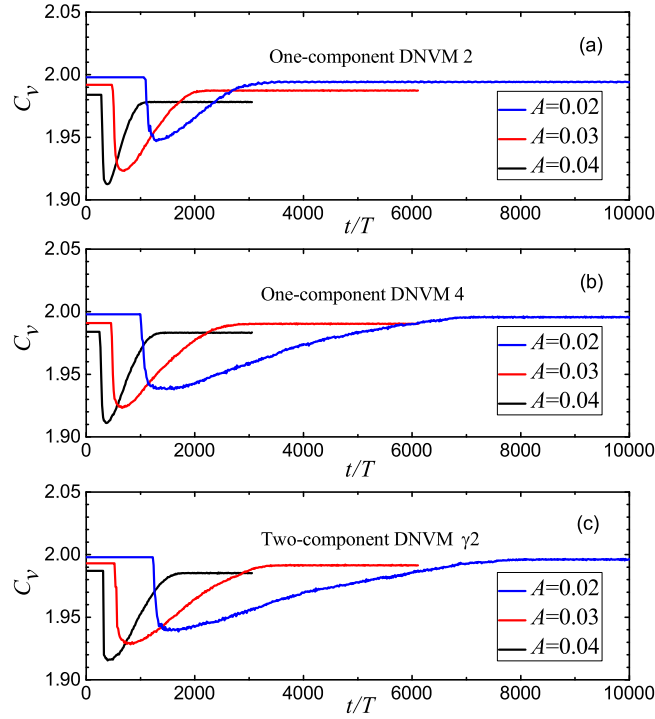


Fig. 6. The ratio of the total to the time-averaged kinetic energy, Eq. (14), as the function of time for (a) DNVM 2, (b) DNVM 4 and (c) DNVM γ_2 . Time is normalized to the period of phonon with maximal frequency, which is close to the period of DB. The blue, red and black curves show the results for $A = 0.02, 0.03$ and 0.04 , respectively.

Averaged over time mean stress, Eq. (19), is presented in Fig. 7 as the function of time for (a) DNVM 2, (b) DNVM 4 and (c) DNVM γ_2 . The mean stress is normalized to the value at thermal equilibrium, $\langle \bar{p} \rangle$. The blue, red and black curves show the results for $A = 0.02, 0.03$ and 0.04 , respectively. The computational cell area in our simulations is fixed, and the tendency to expand is compensated by the appearance of a positive mean stress in the system. However, the mean stress is higher in the thermal equilibrium regime than in the regime of chaotic DBs. We conclude that DBs reduce pressure in the lattice at constant area and hence reduce the thermal expansion of the lattice.

Finally, in Fig. 8, the averaged over time stiffness of the lattice, Eq. (20), is analyzed being normalized to the value at thermal equilibrium, $\langle \bar{C} \rangle$. The results are presented for (a) DNVM 2, (b) DNVM 4 and (c) DNVM γ_2 . In all cases $A = 0.02$. It can be seen that DBs reduce stiffness of the lattice because $\langle \bar{C} \rangle$ increase during the transition from the regime of chaotic DBs to thermal equilibrium. Note that the regime of chaotic DBs for $A = 0.02$ starts at about $t/T = 1200$, when a sharp increase in the localization parameter is observed, see Fig. 3.

6. Discussion and conclusions

Using molecular dynamics simulations, it was demonstrated that the three DNVMs shown in Fig. 1 create chaotic DBs in the triangular β -FPUT lattice as the modulation instability of DNVMs develops. This is because DNVMs have frequencies above the phonon spectrum (see Fig. 2), so they cannot excite extended phonons and the energy is localized on DBs. DBs in the lattice under consideration have a hard-type anharmonicity [40].

The formation of chaotic DBs was proved by monitoring the localization parameter (see Fig. 3), maximal energy of particles (Fig. 4) and distribution of energy over the computational cell (Fig. 5). DBs had a long lifetime, thousands of oscillation periods (see Fig. 3), but over time they disappeared, emitting energy in the form of low-amplitude phonons.

The ratio of the total to kinetic energy, Eq. (14), averaged over time mean stress, Eq. (19), and averaged over time stiffness of the lattice, Eq. (20), were calculated during the transition of the system from the regime with DB to thermal equilibrium (the results are shown in Figs. 6, 7 and 8, respectively). It was found that during this transition the total to kinetic energy ratio, mean stress and stiffness increased. As a result, it was concluded that the hard-type anharmonicity DBs reduce all three investigated macroscopic properties of the lattice. Similar conclusion was made for chaotic DBs in nonlinear chains with the hard-type anharmonicity [27,28], but for the soft-type anharmonicity the effect of DBs on the macroscopic properties is just the opposite [27].

In our simulations the area of the computational cell was constant. Increase in mean stress (pressure) at constant volume means that the lattice tends to expand. In other words, one can say that the hard-type anharmonicity DBs reduce

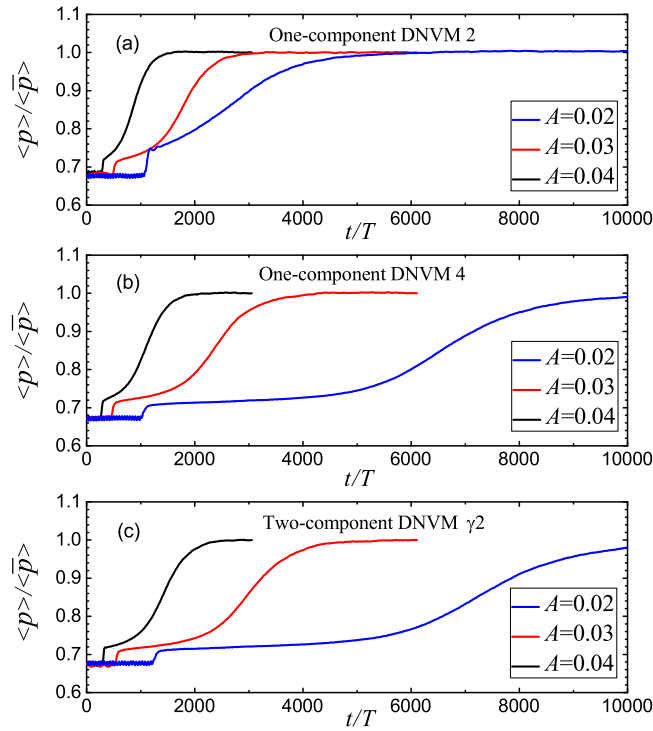


Fig. 7. Averaged over time mean stress, Eq. (19), as the function of time for (a) DNVM 2, (b) DNVM 4 and (c) DNVM γ_2 . The means stress is normalized to the value at thermal equilibrium; time is normalized to the period of phonon with maximal frequency, which is close to the period of DB. The blue, red and black curves show the results for $A = 0.02, 0.03$ and 0.04 , respectively.

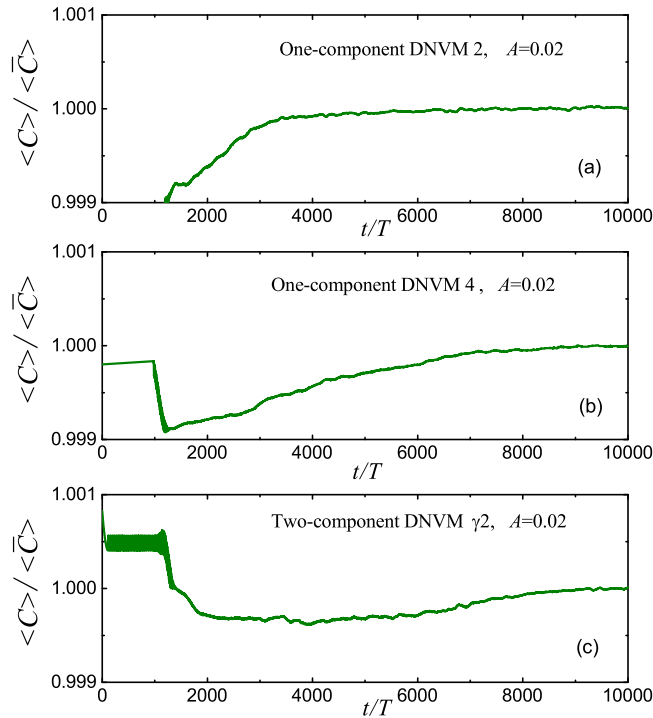


Fig. 8. Averaged over time stiffness of the lattice, Eq. (20), as the function of time for (a) DNVM 2, (b) DNVM 4 and (c) DNVM γ_2 . The stiffness is normalized to the values at thermal equilibrium; time is normalized to the period of phonon with maximal frequency, which is close to the period of DB. Results for $A = 0.02$.

thermal expansion of the lattice because pressure in the lattice at constant volume is smaller in the regime of chaotic DBs and higher in thermal equilibrium.

Similarly, a decrease in the ratio of the total to kinetic energy of the lattice due to excitation of DBs can be associated with a decrease in the specific heat of the lattice. Indeed, specific heat at constant volume is defined as

$$C_v = \lim_{\Delta T \rightarrow 0} \frac{\Delta H}{\Delta T}, \quad (22)$$

where ΔH and ΔT are the total energy and temperature increments, respectively. Temperature increment is proportional to the kinetic energy increment. Suppose in a nonlinear lattice a larger part of total energy increment goes into the form of kinetic energy. This will lead to a faster growth of denominator in Eq. (22) and C_v will decrease. Actually, this happens for the hard-type anharmonicity lattice considered in the present work. Excitation of hard-type anharmonicity DBs results in increase of oscillation frequency and hence in increase of particle velocities and kinetic energy (or temperature) of the system. This is related to a decrease in C_v . System with a soft-type anharmonicity shows an opposite effect, DBs would reduce C_v . A relation between the heat capacity at constant volume and the ratio of the total energy to the kinetic energy has been discussed in the works [27,28,42–44].

DBs affect various macroscopic properties of the lattice with different strengths. The most sensitive to the presence of DBs is the pressure, which in the presence of DBs is approximately 30% lower than at thermal equilibrium (see Fig. 7). The ratio of the total energy to the kinetic energy in the regime of chaotic DBs decreases by about 3% (see Fig. 6), and the tensile rigidity by only 0.1% see Fig. 8.

We hope that our results will stimulate further studies of the effect of discrete breathers on the macroscopic properties of nonlinear lattices, including crystal lattices.

In future studies, we plan to analyze the effect of discrete breathers on the macroscopic properties of three-dimensional model lattices and crystals.

A possible future extension of this work is the inclusion of long-range interactions [45,46]. In this case, employment of a fast particle method like the Barnes–Hut algorithm [47] will allow to reduce the computational cost significantly.

CRedit authorship contribution statement

A. Upadhyaya: Methodology, Investigation. **M.N. Semenova:** Visualization. **A.A. Kudreyko:** Discussions. **S.V. Dmitriev:** Conceptualization, Writing – original draft.

Declaration of competing interest

The authors declare that they have no known competing financial interests or personal relationships that could have appeared to influence the work reported in this paper.

Acknowledgments

For M.N.S. the reported study was funded by the North-Eastern Federal University (NEFU), Russia, contract number 261-02/21 (computer simulations). The work of S.V.D. (discussions, writing the manuscript) was supported by the Russian Science Foundation, Grant No. 21-12-00229.

References

- [1] Dolgov AS. On localization of oscillations in nonlinear crystal structure. *Sov Phys—Solid State* 1986;28:907.
- [2] Sievers AJ, Takeno S. Intrinsic localized modes in anharmonic crystals. *Phys Rev Lett* 1988;61:970.
- [3] Flach S, Willis CR. Discrete breathers. *Phys Rep* 1998;295:181.
- [4] Flach S, Gorbach AV. Discrete breathers - Advances in theory and applications. *Phys Rep* 2008;467:1.
- [5] Dmitriev SV, Korznikova EA, Baimova JA, Velarde MG. Discrete breathers in crystals. *Phys Usp* 2016;59:446.
- [6] Manley ME, Yethiraj M, Sinn H, Volz HM, Alatas A, Lashley JC, et al. Formation of a new dynamical mode in α -uranium observed by inelastic X-ray and neutron scattering. *Phys Rev Lett* 2006;96:125501.
- [7] Manley ME, Yethiraj M, Sinn H, Volz HM, Alatas A, Lashley JC, et al. Intrinsically localized vibrations and the mechanical properties of α -uranium. *J Alloy Compd* 2007;444:129.
- [8] Manley ME, Sievers AJ, Lynn JW, Kiselev SA, Agladze NI, Chen Y, et al. Intrinsic localized modes observed in the high-temperature vibrational spectrum of NaI. *Phys Rev B* 2009;79:134304.
- [9] Manley ME, Abernathy DL, Agladze NI, Sievers AJ. Symmetry-breaking dynamical pattern and localization observed in the equilibrium vibrational spectrum of NaI. *Sci Rep* 2011;1:4.
- [10] Liang W, Vanacore GM, Zewail AH. Observing (non)linear lattice dynamics in graphite by ultrafast Kikuchi diffraction. *Proc Natl Acad Sci U S A* 2014;111:5491.
- [11] Manley ME, Hellman O, Shulumba N, May AF, Stonaha PJ, Lynn JW, et al. Intrinsic anharmonic localization in thermoelectric PbSe. *Nature Commun* 2019;10:1928.
- [12] Kiselev SA, Sievers AJ. Generation of intrinsic vibrational gap modes in three-dimensional ionic crystals. *Phys Rev B* 1997;55:5755.
- [13] Kinoshita Y, Yamayose Y, Doi Y, Nakatani A, Kitamura T. Selective excitations of intrinsic localized modes of atomic scales in carbon nanotubes. *Phys Rev B* 2008;77:024307.
- [14] Khadeeva LZ, Dmitriev SV. Discrete breathers in crystals with NaCl structure. *Phys Rev B* 2010;81:214306.

- [15] Barani E, Korznikova EA, Chetverikov AP, Zhou K, Dmitriev SV. Gap discrete breathers in strained boron nitride. *Phys Lett A* 2017;381.
- [16] Riviere A, Lepri S, Colognesi D, Piazza F. Wavelet imaging of transient energy localization in nonlinear systems at thermal equilibrium: The case study of NaI crystals at high temperature. *Phys Rev B* 2019;99:024307.
- [17] Haas M, Hizhnyakov V, Shelkan A, Klopov M, Sievers AJ. Prediction of high-frequency intrinsic localized modes in Ni and Nb. *Phys Rev B* 2011;84:144303.
- [18] Bachurina OV. Linear discrete breather in fcc metals. *Comp Mater Sci* 2019;160:217.
- [19] Zakharov PV, Korznikova EA, Dmitriev SV, Ekomasov EG, Zhou K. Surface discrete breathers in Pt₃Al intermetallic alloy. *Surf Sci* 2019;679:1.
- [20] Krylova KA, Lobzenko IP, Semenov AS, Kudreyko AA, Dmitriev SV. Spherically localized discrete breathers in bcc metals V and Nb. *Comp Mater Sci* 2020;180:109695.
- [21] Bachurina OV, Kudreyko AA. Two-dimensional discrete breathers in fcc metals. *Comp Mater Sci* 2020;182:109737.
- [22] Chechin GM, Dmitriev SV, Lobzenko IP, Ryabov DS. Properties of discrete breathers in graphane from ab initio simulations. *Phys Rev B* 2014;90:045432.
- [23] Lobzenko IP, Chechin GM, Bezuglova GS, Baimova YA, Korznikova EA, Dmitriev SV. Ab initio simulation of gap discrete breathers in strained graphene. *Phys Solid State* 2016;58:633.
- [24] Manley ME. Impact of intrinsic localized modes of atomic motion on materials properties. *Acta Mater* 2010;58:2926.
- [25] Xiong D, Saadatmand D, Dmitriev SV. Crossover from ballistic to normal heat transport in the ϕ^4 lattice: If nonconservation of momentum is the reason, what is the mechanism? *Phys Rev E* 2017;96:042109.
- [26] Wang J, Dmitriev SV, Xiong D. Thermal transport in long-range interacting Fermi-Pasta-Ulam chains. *Phys Rev Research* 2020;2:013179.
- [27] Singh M, Morkina AY, Korznikova EA, Dubinko VI, Terentiev DA, Xiong D, et al. Effect of discrete breathers on the specific heat of a nonlinear chain. *J Nonlinear Sci* 2021;31:12.
- [28] Korznikova EA, Morkina AY, Singh M, Krivtsov AM, Kuzkin VA, Gani VA, et al. Effect of discrete breathers on macroscopic properties of the Fermi-Pasta-Ulam chain. *Eur Phys J B* 2020;93:123.
- [29] Burlakov VM, Kiselev S. Molecular-dynamics simulation of the decay kinetics of uniform excitation of an anharmonic 1D chain. *Sov Phys-JETP* 1991;72:854.
- [30] Mirnov VV, Lichtenberg AJ, Guclu H. Chaotic breather formation, coalescence, and evolution to energy equipartition in an oscillatory chain. *Physica D* 2001;157:251.
- [31] Ullmann K, Lichtenberg AJ, Corso G. Energy equipartition starting from high-frequency modes in the Fermi-Pasta-Ulam β oscillator chain. *Phys Rev E* 2000;61:2471.
- [32] Kosevich YuA, Lepri S. Modulational instability and energy localization in anharmonic lattices at finite energy density. *Phys Rev B* 2000;61:299.
- [33] Cretegnny T, Dauxois T, Ruffo S, Torcini A. Localization and equipartition of energy in the β -FPU chain: Chaotic breathers. *Physica D* 1998;121:109.
- [34] Tang B, Deng K. Discrete breathers and modulational instability in a discrete ϕ^4 nonlinear lattice with next-nearest-neighbor couplings. *Nonlinear Dynam* 2017;88:2417.
- [35] Korznikova EA, Bachurin DV, Fomin SYu, Chetverikov AP, Dmitriev SV. Instability of vibrational modes in hexagonal lattice. *Eur Phys J B* 2017;90:23.
- [36] Kavitha L, Mohamadou A, Parasuraman E, Gopi D, Akila N, Prabhu A. Modulational instability and nano-scale energy localization in ferromagnetic spin chain with higher order dispersive interactions. *J Magn Magn Mat* 2016;404:91.
- [37] Kavitha L, Parasuraman E, Gopi D, Prabhu A, Vicencio RA. Nonlinear nano-scale localized breather modes in a discrete weak ferromagnetic spin lattice. *J Magn Magn Mat* 2016;401:394.
- [38] Ikeda K, Doi Y, Feng BF, Kawahara T. Chaotic breathers of two types in a two-dimensional Morse lattice with an on-site harmonic potential. *Physica D* 2007;225:184.
- [39] Ryabov DS, Chechin GM, Upadhyaya A, Korznikova EA, Dubinko VI, Dmitriev SV. Delocalized nonlinear vibrational modes of triangular lattices. *Nonlinear Dynam* 2020;102:2793.
- [40] Babicheva RI, Semenov AS, Soboleva EG, Kudreyko AA, Zhou K, Dmitriev SV. Discrete breathers in a triangular β -Fermi-Pasta-Ulam-Tsingou lattice. *Phys Rev E* 2021;103:052202.
- [41] Bakhvalov NS. Numerical methods: Analysis, algebra, ordinary differential equations. Moscow: MIR Publishers; 1977.
- [42] Velarde MG, Ebeling W, Chetverikov AP. Thermal solitons and solectrons in 1d anharmonic lattices up to physiological temperatures. *Int J Bifurcation Chaos* 2008;18:3815.
- [43] Chetverikov AP, Ebeling W, Velarde MG. Dissipative solitons and complex currents in active lattices. *Int J Bifurcation Chaos* 2006;16:1613.
- [44] Chetverikov AP, Ebeling W, Velarde MG. Dissipative solitons and complex currents in active lattices. *Int J Bifurcation Chaos* 2006;16:1613.
- [45] Christodoulidi H, Tsallis C, Bountis T. Fermi-Pasta-Ulam model with long-range interactions: Dynamics and thermostatics. *Europhys Lett* 2014;108:40006.
- [46] Wang J, Dmitriev SV, Xiong D. Thermal transport in long-range interacting Fermi-Pasta-Ulam chains. *Phys Rev Res* 2020;2:013179.
- [47] Barnes J, Hut P. A hierarchical O(N log N) force-calculation algorithm. *Nature* 1986;324:446.